Holocene palaeoenvironmental conditions in NE Bulgaria uncovered by mineral magnetic and paleomagnetic records of an alluvial soil

Diana Jordanova, Bozhurka Georgieva, Neli Jordanova, Yohan Guyodo, France Lagroix

Quaternary International 631 (2022) 47–58

Contents lists available at ScienceDirect

Quaternary International

journal homepage: www.elsevier.com/locate/quaint

Holocene palaeoenvironmental conditions in NE Bulgaria uncovered by mineral magnetic and paleomagnetic records of an alluvial soil

Diana Jordanova [a,*], Bozhurka Georgieva [a], Neli Jordanova [a], Yohan Guyodo [b], France Lagroix [b]

[a] National Institute of Geophysics, Geodesy and Geography, Bulgarian Academy of Sciences, Acad. G. Bonchev, bl.3, 1113, Sofia, Bulgaria
[b] Université Paris Cité, Institut de Physique du Globe de Paris, CNRS, 1 rue Jussieu, 75005, Paris, France

ARTICLE INFO

Keywords:
Alluvial soil
Paleomagnetism
Archaeological age constrains
Paleoclimate
Holocene

ABSTRACT

Retrieving well-dated terrestrial archives of Holocene climate change is fundamentally important for building robust climate models and predictions. In this study we obtained records of paleomagnetic direction and relative paleointensity of the Earth's magnetic field from an alluvial soil situated on a flood river terrace close to the well-dated and stratigraphically confined Chalcolithic mound near the village of Koprivetz in NE Bulgaria. Anisotropy of magnetic susceptibility data revealed a coherent imbricated magnetic fabric reflecting the effects of water flow in the lower alluvial clays and the direction of delluvial sedimentation from the slope in the upper soil horizons. Variations of declination, inclination and relative paleointensity along depth of the soil profile were correlated to the archaeomagnetic secular variation curves for Bulgaria, using the age of the earliest archaeological stratigraphic horizon as the main tie point. Based on this correlation, an age model was constructed and temporal variations of environmental magnetic parameters were examined for their suitability as paleoclimate proxies. The ratio of frequency dependent susceptibility to anhysteretic susceptibility (χ_{fd}/χ_{ARM}) is a reasonable proxy for paleoprecipitation due to its close resemblance to paleo-flood records from the Northern and Southern Alps. Events of increased flood intensities during the late Holocene (post – 4700 y BP) are registered through χ_{fd}/χ_{ARM} and reveal good correspondence to the flood records of rivers in Southern Alps and Carpathians. The ratio of isothermal remanent magnetization after 20 mT alternating field demagnetization (IRM_{20mT}) normalized to the full IRM showed good consistency with the GISP2 ice record of temperature variations in Greenland during the Holocene. Six major cold incidents during the last 7000 y BP with the major one at 4500 y BP are evidenced. The obtained results suggest that climate at mid-latitude SE Europe is sensitive to the changes in North Atlantic circulation.

1. Introduction

Changes in Holocene palaeoenvironments and climate played a crucial role in the lateral spread, pathways, and evolution of human societies (Weninger et al., 2009, 2014; Berger, 2021). The Balkans represent a central root for the Neolithic spread, which had started at about 9000 y BP from Anatolia to Southern Europe (Greece) towards central and western Europe (Bogucki, 1996; Weninger et al., 2009; Fort, 2015). On the other hand, anthropogenic forcing on the environment is evident in SE Europe since the beginning of forest clearance about 2500 y BP (Feurdean et al., 2021). This continuing human – environment interaction resulted in significant anthropogenically induced rise in greenhouse gas emissions and related warming (Ruddiman et al., 2016). Thus, revealing the history of paleoenvironmental changes from a variety of interdisciplinary proxies is a valuable approach in evolutionary studies.

The aim of the present investigation is to reveal the influence of natural and anthropogenic factors in the history of Holocene environmental changes in southeastern Europe from the mineral magnetic record of an alluvial soil sampled near one of the oldest Neolithic settlements in Bulgaria (Koprivetz). Moreover, we show that this soil profile reliably recorded the behavior of the Earth's magnetic field (declination (D), inclination (I) and relative paleointensity (RPI)) during the last 8000 years BP.

2. Regional setting

In a regional plan, the study site is located in SE Europe (Fig. 1). The

* Corresponding author.
E-mail address: diana_jordanova77@abv.bg (D. Jordanova).

https://doi.org/10.1016/j.quaint.2022.06.009
Received 23 January 2022; Received in revised form 14 June 2022; Accepted 16 June 2022
Available online 30 June 2022

European climate is strongly influenced by the dynamics of the storm tracks, which bring moisture to the continent from North Atlantic ocean (Brayshaw et al., 2010). Thus, hydroclimate and river water fluctuations at millennial time scales also respond to these external forces and can be sensitively recorded by fluvial sedimentary successions (Macklin et al., 2012).

The studied soil profile is located in Northeastern Bulgaria, about 50 km south from the Danube River (Fig. 2a). The sampling site Koprivetz (KP) (43°24′30″N, 25°53′35″E) is situated on the flood terrace T_0 of the Baniska River, flowing north to the Danube (Fig. 2b). Steep slope towards the plateau to the west from the sampling location is a landform supplying delluvial material to the river flood terrace (Fig. 2 b, c). The positions in the landscape of the archaeological sites near Koprivetz are clearly linked to changing environmental conditions during the respective period as described by Evlogiev (2006). The oldest settlement is found on the third river terrace T_3 (Fig. 2c). It consists of four horizons of the Early Neolithic period in NE Bulgaria. The stratigraphic position of the oldest Early Neolithic horizon is found in the uppermost part of the last glacial loess L_1. On the slope towards the third river terrace (T_3) a Late Neolithic settlement is found. It consists of four stratigraphic horizons, with the oldest one constructed in the delluvial loess. The youngest Chalcolithic mound is located on the flood terrace T_0 of the Baniska River (Fig. 2c). Ancient inhabitants moved there after the river retreated to its present day position. Five horizons of Chalcolithic age were identified in an archaeological trench (Popov, 1996). The oldest stratigraphic horizon of the Chalcolithic mound is dated at 6000 y BP and extends down to 140 cm depth. It is marked by sandstone plates horizontally laid by ancient inhabitants. These plates were most probably utilized to prevent sinking in the mud of the floodplain clays during village construction (Popov, 1996).

3. Materials and methods

3.1. Sampling

A profile of an alluvial soil was sampled near the Chalcolithic mound (Fig. 2b). The profile consists of a humic horizon (Ah) in the uppermost 10 cm, followed by 135 cm thick transitional horizon (A/C). The parent material (C horizon) is represented by grey alluvial clays and was sampled down to 200 cm depth. Oriented samples were gathered continuously at each 3 cm depth using small stainless steel core samplers with 2 × 2 cm square cross-section and 10 cm length. The samplers were pressed and gently hammered perpendicularly to the cleaned vertical wall of the outcrop. Azimuth of the core with respect to the geographic north is noted and the dip is kept zero with this sampling design. From each core 1 or 2 oriented samples of 2 × 2 × 2 cm dimensions were cut. The collection of oriented samples consists of 123 cubes.

3.2. Laboratory measurements

Anisotropy of magnetic susceptibility (AMS) of all samples was measured on MFK-1A kappabridge (AGICO, Czech Republic) using an

Fig. 1. Study area (marked as black rectangle) in a regional context (map reused from Europe relief map, 2010).

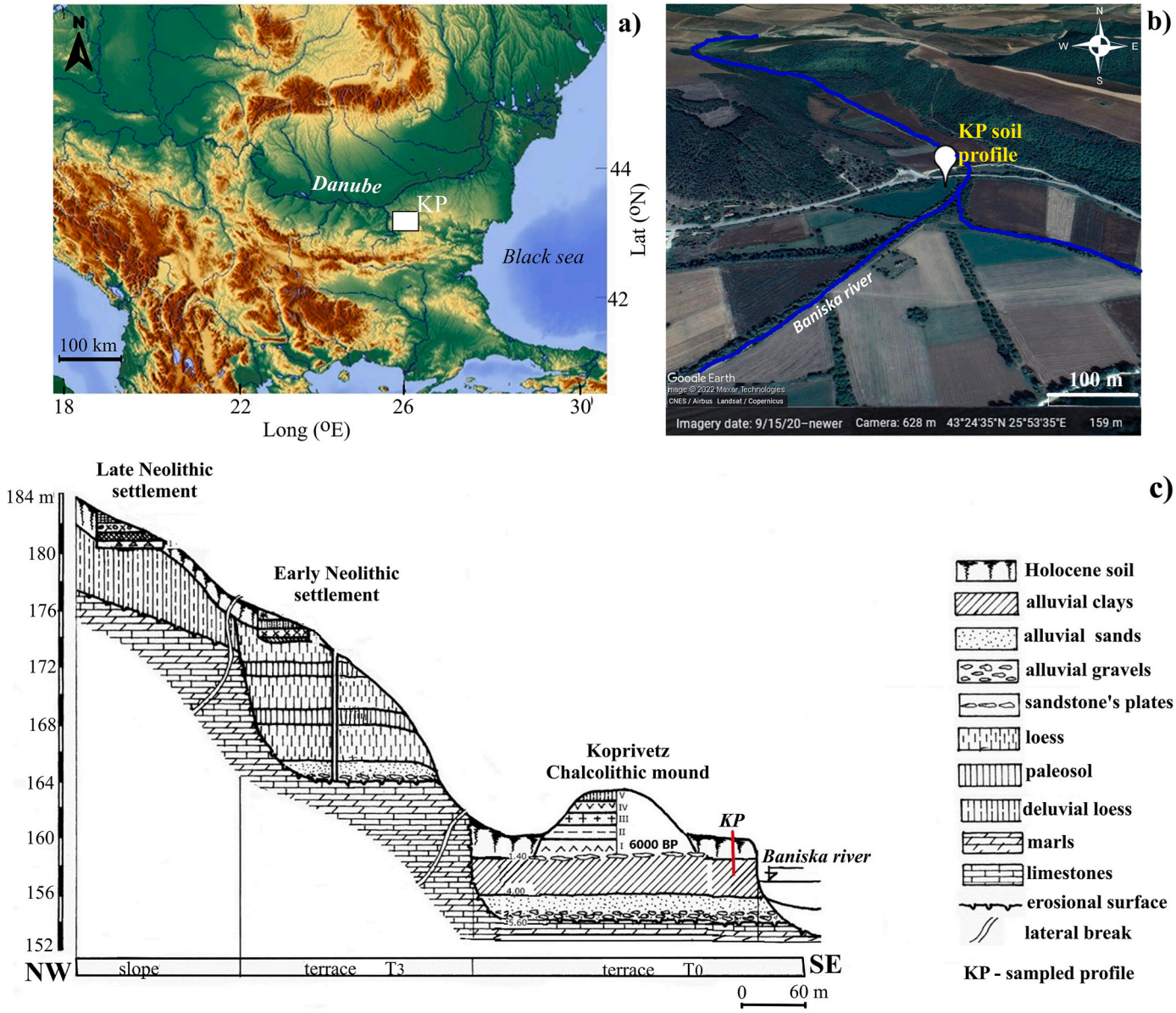

Fig. 2. (a) Location of Koprivetz (KP) site (indicated by white rectangle) in the lower Danube area (map from MFF maps (Braxmeier, 2017); b) map showing the position in the landscape of the sampled soil profile KP (shown by the white symbol). Map created in Google Earth (2022). Nearby Neolithic village is positioned at the slope of the hill from northwest and the Chalcolithic mound is next to the sampled soil profile at the flood terrace of Baniska river; c) geological section of the site (modified after Evlogiev, 2006).

automated rotator. Mean magnetic susceptibility (K_{mean}), AMS tensor (principal directions of maximum K_{max}, intermediate K_{int} and minimum K_{min} susceptibility axes) and a set of the main AMS parameters (lineation L, foliation F, corrected degree of anisotropy Pj, shape factor T) (Hrouda, 1982) were obtained using the ANISOFT program (AGICO). Magnetic lineation (L) is defined as

$$L = \left(\frac{K_{max}}{K_{int}}\right)$$

Magnetic foliation (F) is given by the ratio:

$$F = \left(\frac{K_{int}}{K_{min}}\right)$$

Corrected degree of anisotropy (Pj) is introduced by Jelinek (1981) as:

$$P_j = exp\sqrt{\{2[(\eta_1 - \eta_m)^2 + (\eta_2 - \eta_m)^2 + (\eta_3 - \eta_m)^2]\}}$$

where $\eta_1 = \ln(K_{max})$, $\eta_2 = \ln(K_{int})$, $\eta_3 = \ln(K_{min})$ and $\eta_m = (\eta_1\eta_2\eta_3)^{1/3}$

Shape parameter (T) evaluates the shape of AMS ellipsoid independent on the degree of anisotropy and is calculated according to the formula:

$$T = \left[\frac{2(\eta_2 - \eta_3)}{(\eta_1 - \eta_3)}\right] - 1 = \frac{ln(F) - ln(L)}{ln(F) + ln(L)}$$

Extreme cases are T-values of zero (T = 0) signifying isotropic shape (sphere); T = 1 stands for oblate ellipsoid (disc shape), and T = −1 characterizes elongated ellipsoids (rod – shape) (Jelinek, 1981).

For evaluation of the statistical significance of the directional AMS results, uncertainly ellipses (ε) around the principal anisotropy axes K_{max}, K_{int}, K_{min} are defined and labelled by numbers 1, 2, and 3. At single specimen level ε12 represents 95% confidence ellipse uncertainty of

K_{max} within the magnetic foliation plane. To consider K_{max} direction as statistically significant, maximum allowable ε12 is 22.5°. A statistically significant magnetic foliation is considered as one for samples with e23 < 30° (Lagroix and Banerjee, 2004).

Additionally, bulk magnetic susceptibility (χ) of the samples was measured at two frequencies - 976 Hz and 15616 Hz - in a 200 A/m magnetic field. Frequency-dependent magnetic susceptibility $\chi_{fd} = (\chi_{lf} - \chi_{hf})$ was calculated.

The experimental set up and paleomagnetic study were carried out following the classical approach in sediment's magnetostratigraphy (Stoner and St-Onge, 2007). Natural remanent magnetization (NRM) of 66 samples (one per depth interval) was measured at the Paleomagnetic Laboratory of the Institut de Physique du Globe de Paris (IPGP) (France) in a magnetically shielded room using a 755-R SRM 2G cryogenic magnetometer. AF demagnetization was carried out on an ASC Scientific D-2000 AF-demagnetizer/magnetizer along the three orthogonal sample axes consecutively. Eleven samples were chosen for detailed AF-demagnetization in 11 steps with peak amplitudes of 5, 10, 20, 30, 40, 50, 60, 80, 100, 150 and 200 mT. Demagnetization results were analyzed by principal component analysis (PCA) for determination of the characteristic remanent magnetization (ChRM) using the REMASOFT software (AGICO, Czech Republic). Based on the results from these 11 pilot demagnetizations, the remaining 55 samples were AF demagnetized in 4 steps (peak amplitudes of 20, 30, 40 mT and 50 mT). Median destructive field (MDF) of NRM was determined from the demagnetization curve. Anhysteretic remanent magnetizations (ARM) were imparted with an AF peak amplitude of 100 mT superimposed on a 50 μT static direct current (DC) field along the samples z-axis. Anhysteretic susceptibility was calculated as ARM normalized by the amplitude of the weak DC field. ARM acquired by the 11 pilot samples was stepwise AF demagnetized at the same steps as for NRM demagnetization. The remaining 55 samples were AF demagnetized using a peak AF amplitude of 20 mT and used to determine the relative paleointensity (RPI). Isothermal remanent magnetization (IRM) was imparted using a MMPM10 pulse magnetizer (Magnetic Measurements Ltd, UK) at 1T field. All samples were AF demagnetized afterwards at 20 mT peak field.

The ratios NRM_{20mT}/χ, NRM_{20mT}/ARM_{20mT} and NRM_{20mT}/IRM_{20mT} were tested for their suitability for being a proxy of relative paleointensity (RPI) of the geomagnetic field (Tauxe, 1993). As far as the soil formation process developed in the alluvial/delluvial sediments, their ChRM is of detrital origin. A correction for the effect of grain size variations on detrital remanent magnetization (DRM) is made for NRM_{20mT}/ARM_{20mT} ratio according to the method, proposed by Brachfeld and Banerjee (2000). The consistency between this choice of RPI proxy and the commonly utilized slope method for RPI determination is checked by determining the slope coefficient for the 11 samples with NRM and ARM detailed stepwise demagnetization data.

For further refinement of the RPI proxy and elimination of possible grain size effects, reflected by variations in MDF_{NRM}, we applied the procedure described in Brachfeld and Banerjee (2000). This additional correction is made according to the expression:

$$RPI' = RPI * MDF_{NRM\text{-}CM} / MDF_{NRM}$$

where $MDF_{NRM\text{-}CM}$ is the center of mass of the MDF_{NRM}. The latter is determined from the RPI vs. MDF_{NRM} scatter plot.

Diagnostic mineral magnetic measurements for the identification of magnetic carriers relay on the detection of Curie and/or Neel temperatures, which are uniquely characterizing certain ferri(antiferro)magnetic oxides (Dunlop and Özdemir, 1997). For that purpose we carried out thermomagnetic analysis of magnetic susceptibility using a high-temperature furnace CS-2 to the Kappabridge KLY-2 at Sofia Paleomagnetic Laboratory. Heating and cooling cycles from room temperature to 700 °C were performed in air at a heating rate of 11 °C/min. Information on the effective magnetic domain state of the remanence carriers was obtained by hysteresis loops measured on a VSM model 3900 (Princeton Measurements Corporation, USA) at IPGP for 11 samples in a maximum applied field of 1.5T. After correction of the linear slope at high field (>1.05 T), the following hysteresis parameters were retrieved: coercive force (B_c), saturation magnetization (M_s) and saturation remanence (M_r). Coercivity of remanence (B_{cr}) is determined from back-field remagnetization experiment of an initial forward field 1.5 T IRM. Finally, stepwise acquisition of IRM was conducted in 80 logarithmic steps up to 1.5T. IRM acquisition curves were fitted by best-fit combination of log-normal distribution functions using the MaxUnMix software (Maxbauer et al., 2016). The parameters determined are: the mean coercivity of an individual component (B_h), the component saturation magnetic remanence (M_r%) as a percentage of the total remanence, and the dispersion parameter (DP) corresponding to one standard deviation in log space of the component's coercivity distribution.

At Sofia Paleomagnetic Laboratory, all samples were magnetized in a 2T DC field using an ASC IM-10-30 pulse magnetizer (ASC Scientific, USA) in a forward field (IRM_{2T}) and then in a 300 mT backfield (IRM_{-300mT}). The S-ratio was calculated according to King and Channell (1991) as $S = (IRM_{-0.3T}/IRM_{2T})$. Remanences were measured using a JR-6A automatic spinner magnetometer (AGICO Ltd., Czech Rep.) with a sensitivity of 2×10^{-6} A/m.

4. Results

4.1. Identification and characterization of magnetic iron oxides

Thermomagnetic analyses on selected samples from the uppermost 90 cm of the soil profile (Fig. 3A) reveal relatively stable signal until 270 °C, followed by sharp decrease until 450 °C and subsequent susceptibility increase before the final sharp thermal unblocking at 600 °C. The samples from the deeper soil layers (see KP 171 cm in Fig. 3A), not affected by the presence of humic substances do not show the increase of susceptibility during heating higher than 500 °C but only sharp demagnetization after 550 °C with T_c of 580 °C. All samples undergo extensive mineralogical alterations leading to the creation of a magnetite like new phase suggested by the observed 10-fold rise in susceptibility upon cooling (Fig. 3A).

IRM acquisition curves were fitted by four coercivity components (Fig. 3B, Table 1S). Their relative proportion does not change significantly with depth: the lowest coercivity component (component 1, C1) contributes 4–7% of the total IRM and B_h ranges from 2.5 to 4 mT; the second coercivity component (C2) accounts for 62–68% of the total IRM with mean coercivities in the range of 23.2–24.5 mT; component 3 (C3) accounts for 22–27% of the total IRM and has a wider range of coercivities from 85 to 97 mT; component 4 (C4) is characterized by coercivities between 300 and 750 mT and contributes between 2 and 8% to the total IRM.

Behavior of magnetic hysteresis parameters with depth is shown in Fig. 4 a-c. Concentration-dependent saturation magnetization M_s and saturation remanence M_r decrease steadily from the surface Ah and A/C horizon down to 100 cm depth. Small but systematic increase in deeper levels is observed. Coercivity parameters do not show strong variations with B_c and B_{cr} values constrained between 9-10 mT and 26–28 mT respectively. The ratios M_r/M_s and B_{cr}/B_c reveal higher variability in the lower part of the studied profile – in the weakly magnetic grey clay unit. The S-ratio, calculated for all depth levels (Fig. 4d) is characterized by systematic decrease towards the bottom part of the profile from values of 0.96 to 0.7. Variations with depth of the coercivity of the four unmixed IRM components are presented in Fig. 4 e-h and their relative share in the total IRM – in Fig. 1S. The softest component C1 has B_h maximum at 60 cm depth (Fig. 4e), while coercivities of C2, and C4 show the highest values at the near surface horizon and decrease down to 100 cm (Fig. 4 f, h). The share of higher coercivity component C3 increases after 120 cm depth (Fig. 1S) along with its decreasing coercivity (Fig. 4 g). Similarly, the highest contribution from C4 component (Fig. 1S) is attained at the

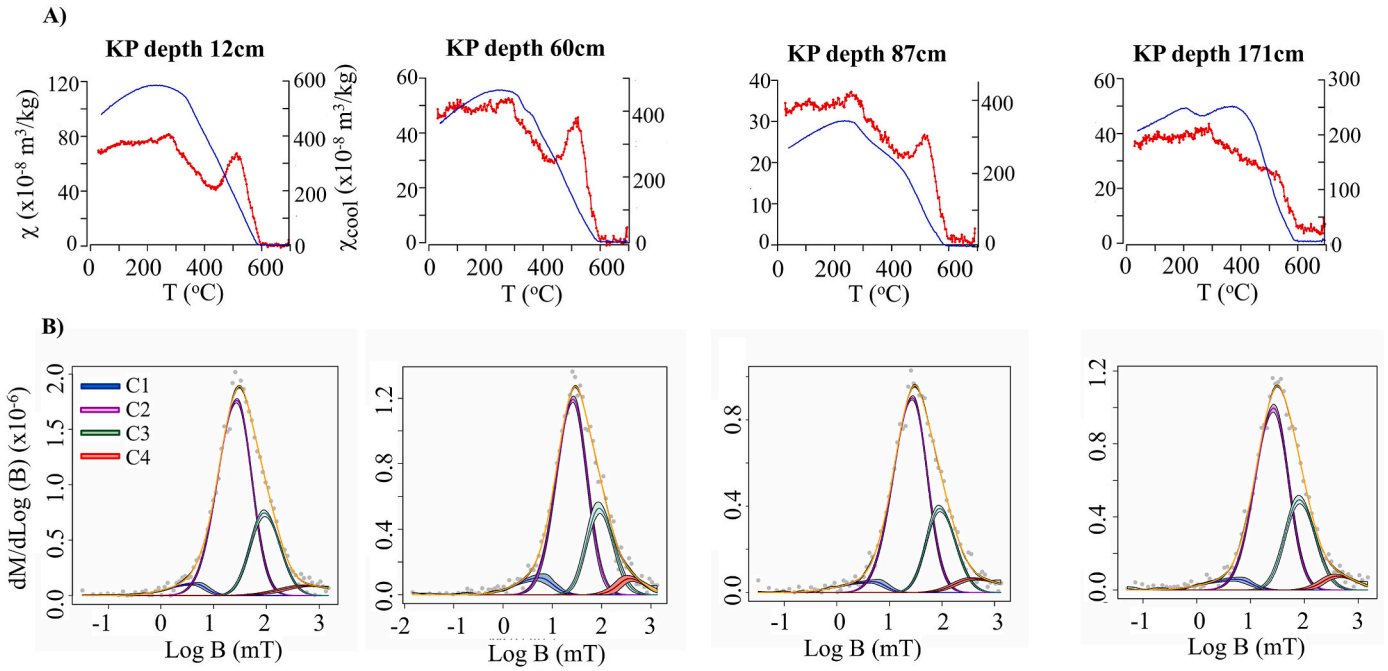

Fig. 3. A) Representative thermomagnetic analyses of magnetic susceptibility (χ(T)) of samples from different depth intervals – heating in air at 11 °C/min; B) Unmixing of IRM stepwise acquisition curves for the same samples shown in (A) using the MaxUnMix software (Maxbauer et al., 2016). Data points are denoted by dots; cumulative fit together with its confidence band is shaded in yellow. Color coding of the fitted components C1, C2, C3 and C4 is given in the left panel of (B). (For interpretation of the references to color in this figure legend, the reader is referred to the Web version of this article.)

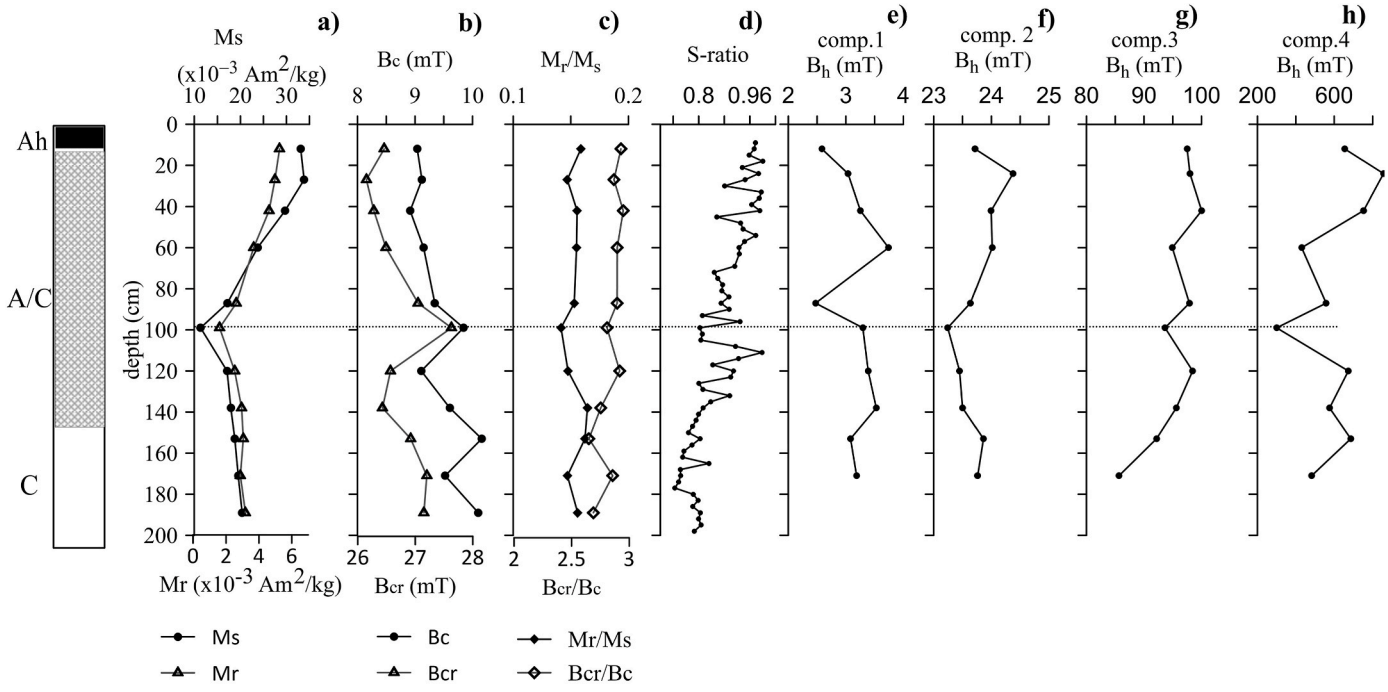

Fig. 4. Depth variations of hysteresis parameters and ratios (a–c); S-ratio (d), and mean coercivities (B_h) of the four IRM components fitted to IRM acquisition curves (e - h). Stratigraphic column with soil horizons is shown on the left.

depth of its minimum B_h value at 100 cm depth (Fig. 4h).

4.2. *Paleomagnetic directions and relative paleointensity estimates*

The NRMs median destructive fields (MDF_{NRM}) range from 10 to 21 mT providing evidence for low coercivity magnetic minerals as carriers of NRM (Fig. 2S b). Examples of stepwise AF demagnetization behavior and NRM components are presented in Fig. 5. For most samples, NRM has two components. The first one is removed after 10–20 mT demagnetization step and is probably of viscous origin. The characteristic NRM component (ChRM) is well defined by a linear segment comprised the 20–50 mT demagnetization steps or up to 80 mT for certain samples. Low maximum angular deviation (MAD) values (<5%) of the ChRM directions are obtained for 88% of the samples with MAD values below

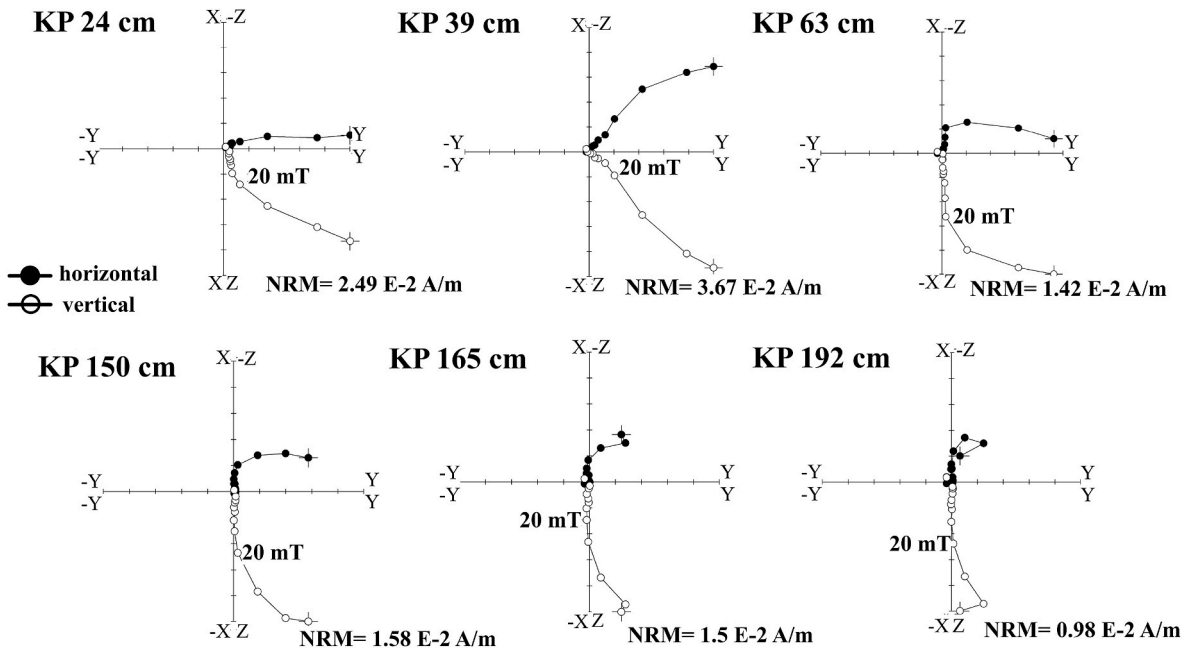

Fig. 5. Orthogonal vector plots of NRM AF stepwise demagnetization. 20 mT step is indicated as the first point of the isolated ChRM.

10% for the remaining samples, except one (see Fig. 2S c). ChRM fit is anchored to the origin of the diagram.

Four samples gave anomalous ChRM declinations and seven samples – anomalous ChRM inclination values. These were rejected and excluded from the analysis. The obtained D and I of the ChRM component vary in the ranges 55–75° for inclination, and −30 to 60° for declination. As proxies for estimation of relative paleointensity (RPI), three ratios were considered: NRM_{20mT}/χ; NRM_{20mT}/IRM_{20mT}, and NRM_{20mT}/ARM_{20mT} (Fig. 2 S d - f). All three show similar variabilities along the soil profile with small differences in the relative amplitude of different peak values.

Coherency tests for possible correlations between the RPI proxy ratio and the normalizer were carried out according to Tauxe and Wu (1990) by using Statistica 8.0 software with Fourier time series analysis tool-pack. The results show some coherency (higher than 0.5) between all normalizers with the corresponding RPI proxy ratio at high frequencies, corresponding mainly to depth intervals of 2.5 – 3 cm, which is in fact close to the sampling interval. This coherency is largely removed after the application of the grain size correction (Fig. 3S).

4.3. Anisotropy of magnetic susceptibility (AMS)

The degree of anisotropy P for all samples studied is low, with maximum values of 1.05. As seen from the bi-plot of foliation vs lineation (Fig. 6 a), foliation is mostly determining the P-values. Further evidence for the oblate shape of the AMS ellipsoid are data for the shape parameter T, showing prevailing positive values (plot not shown). The statistical significance of the directional results are evaluated according to Zhu et al. (2004) and Lagroix and Banerjee (2004). The angular uncertainty in the calculated directions of K_{max} are assessed by ε12 values. All samples except one have ε12 less than 20°, so we applied more stringent criteria and remove samples with ε12 > 11° (Lagroix and Banerjee, 2004). The observed negative correlation between ε12 and lineation L (Fig. 6a) reflects the fact that samples having weaker lineation are prone to higher random uncertainties in the direction of K_{max}. Statistical significance of the calculated magnetic foliation is estimated by ε23 parameter (Zhu et al., 2004). Similar to ε12 – lineation relationship, ε23 shows strong dependence on foliation F (Fig. 6a). At the same time, poor correlation is obtained between ε12 and foliation, and between ε23 and lineation. Stereographic projections of the orientations of principal susceptibility axes (K_{max}, K_{int}, K_{min}) for the upper 145 cm developed in the delluvium (Fig. 6b) and lower depth interval (146–200 cm) represented by alluvial clays (Fig. 6c) reveal significant differences in the observed magnetic fabrics. In the upper Ah and A/C soil horizons (0–145 cm depth), K_{max} axes are preferentially distributed sub-horizontally (mean I-K_{max}) = 2.5°) in the first quadrant (mean D-K_{max} = 23.4°). The foliation is inclined with pole to foliation plane showing mean inclination of 55.2° (mean I-K_{min}). Well-grouped principal susceptibility directions were obtained for the alluvial clays at 146–200 cm depth (Fig. 6c). The orientations of the three principal susceptibility axes, however, are different as compared to the upper part. Again, K_{max} is sub-horizontal with mean azimuth of 158.6° and poles to foliation plane inclined at mean I-K_{min} of 58.9° (Fig. 6c) towards NE (mean D-K_{min} of 66.1°).

Depth variations in the anisotropy parameters and the three principal directions are shown in Fig. 7. The most obvious changes are observed in the inclination of K_{min} axis – the shallowest values are revealed at about 100 cm depth and systematic increase of I-K_{min} towards vertical is obtained from 100 cm upwards. This change is coincident with the onset of increasing bulk volume susceptibility. Similarly, anisotropy parameters (lineation L, foliation F, shape parameter T and the corrected degree of anisotropy Pj) all show higher variability and reach the highest values in the upper 100 cm (Fig. 7 f – i).

5. Discussion

5.1. Mineral magnetic carriers of induced and remanent magnetization along the studied profile

The experimental data on magnetic mineral identification point out to uniform magnetic carriers along the depth of the studied profile. Thermomagnetic analyses of magnetic susceptibility (Fig. 3a) reveal fairly uniform k-T behavior for samples down to 90 cm depth, pointing to the dominance of two strongly magnetic phases – one with T_c or transformation temperature of 270–320 °C, probably maghemite, and second one – typical for oxidized magnetite (T_c of 600 °C) (Dunlop and Özdemir, 1997). The reducing environment induced by organic matter upon heating favors the formation of a strongly magnetic phases (Hanesch et al., 2006). They appear as a result of thermal alteration of non-magnetic clay minerals, goethite, lepidocrocite, and ferrihydrite into strongly magnetic magnetite (Murad and Wagner, 1998; Cornell

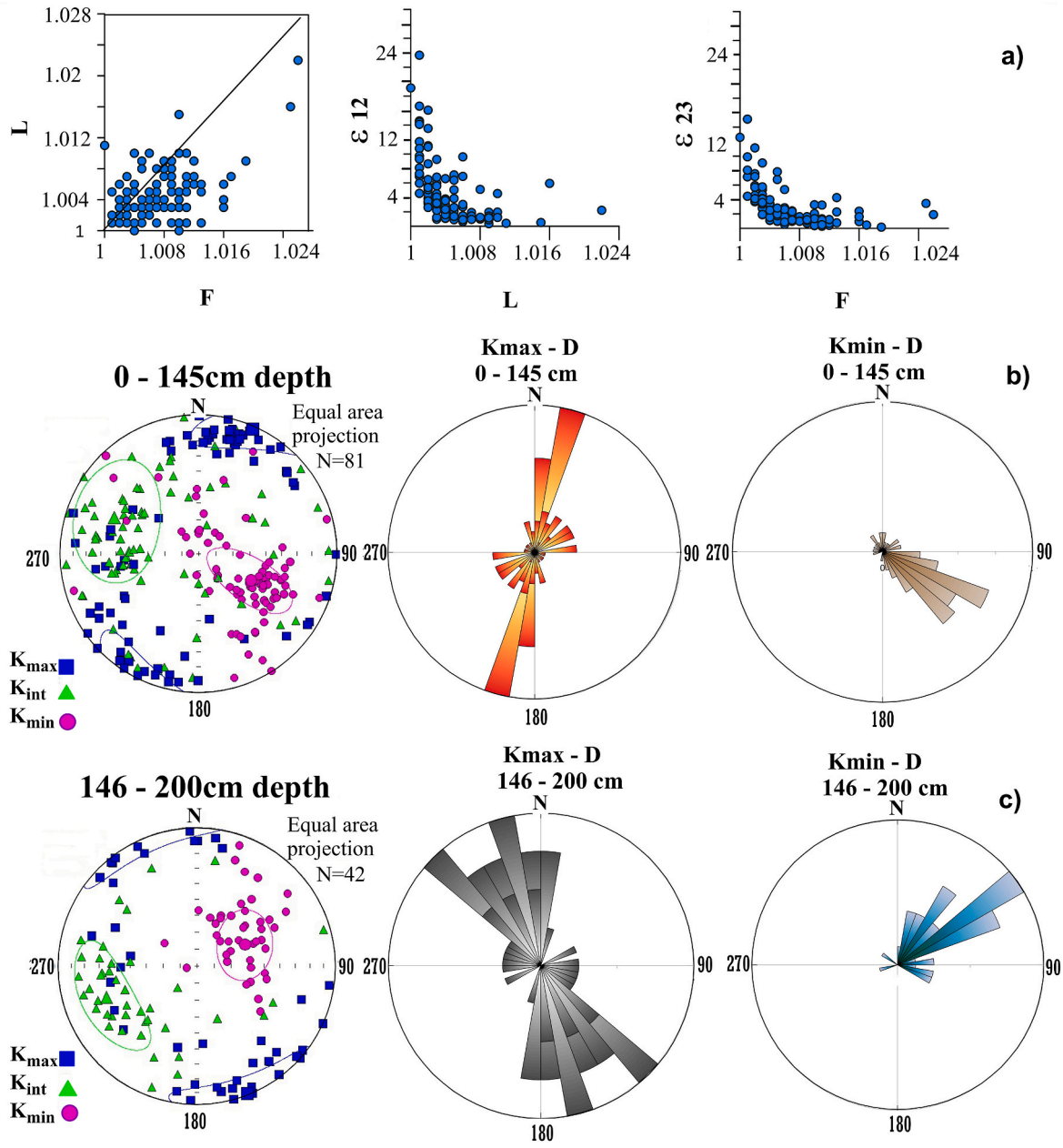

Fig. 6. Results from anisotropy of magnetic susceptibility measurements. A) bi-plots of lineation (L) versus foliation (F); 95% confidence half angle around K_{max} and K_{int} within the K_{max}-K_{int} plane (ε12) versus magnetic lineation L, and around K_{min} and K_{int} within the K_{min}-K_{int} plane (ε23) versus F; b) lower hemisphere stereographic projection (geographic coordinates) of the maximum (K_{max}), intermediate (K_{int}) and minimum (K_{min}) AMS principal axes of samples from the soil Ah and A/C horizons developed in delluvial clays; rose diagram of the K_{max} declinations and plunge of the poles to the imbrication plane (D-K_{min}). c) the same as b) for samples from the alluvial clays in the C horizon.

and Schwertmann, 2003; Hanesch et al., 2006; Till et al., 2014, 2015; Jiang et al., 2015; Ponomar et al. 2020). Such newly created phase most probably unblocks sharply at ~500 °C for samples from 90 cm depth to the surface (Fig. 3a). The absence of the peak at 500 °C on the cooling curve for the sample at 171 cm depth probably indicates deficiency of organic matter, although the strong increase of the signal on cooling as relative percent from the initial susceptibility is similar to that of other samples. Consequently, another source favoring reducing conditions, such as water from the dehydration of hydrous minerals, during heating at high temperatures (above 600 °C) induces similar reactions (Guo and Barnard, 2016). The latter contribute to k-increase on cooling for the soil samples as well.

Further evidences for the type of magnetic minerals carrying the remanent magnetization are complemented by IRM coercivity components unmixing (Fig. 3b). The presence of four different coercivity components imply more complex mineral magnetic carriers than two-phase mixture of strongly magnetic maghemite and magnetite, as suggested by k-T analysis. High-coercivity components with B_h of ~95 mT (comp. C3) and 400–700 mT (comp. C4) and intensities comprising more than a quarter of the total $IRM_{1.5T}$ (Table 1S) suggest that weakly magnetic (antiferromagnetic) iron oxides are also present. These could be either partially magnetized goethite or finer grained hematite. The relative share of C4 component exhibits maximum at 100 cm depth and remains stable in the C-horizon (Fig. 1S).

Downward decrease in coercivity of component C3 especially in the alluvial clays (C-horizon) is observed (Fig. 4g). The most feasible candidate mineral carrier of component C3 is hematite, which is the most thermodynamically stable iron oxide in surface environments (Guo

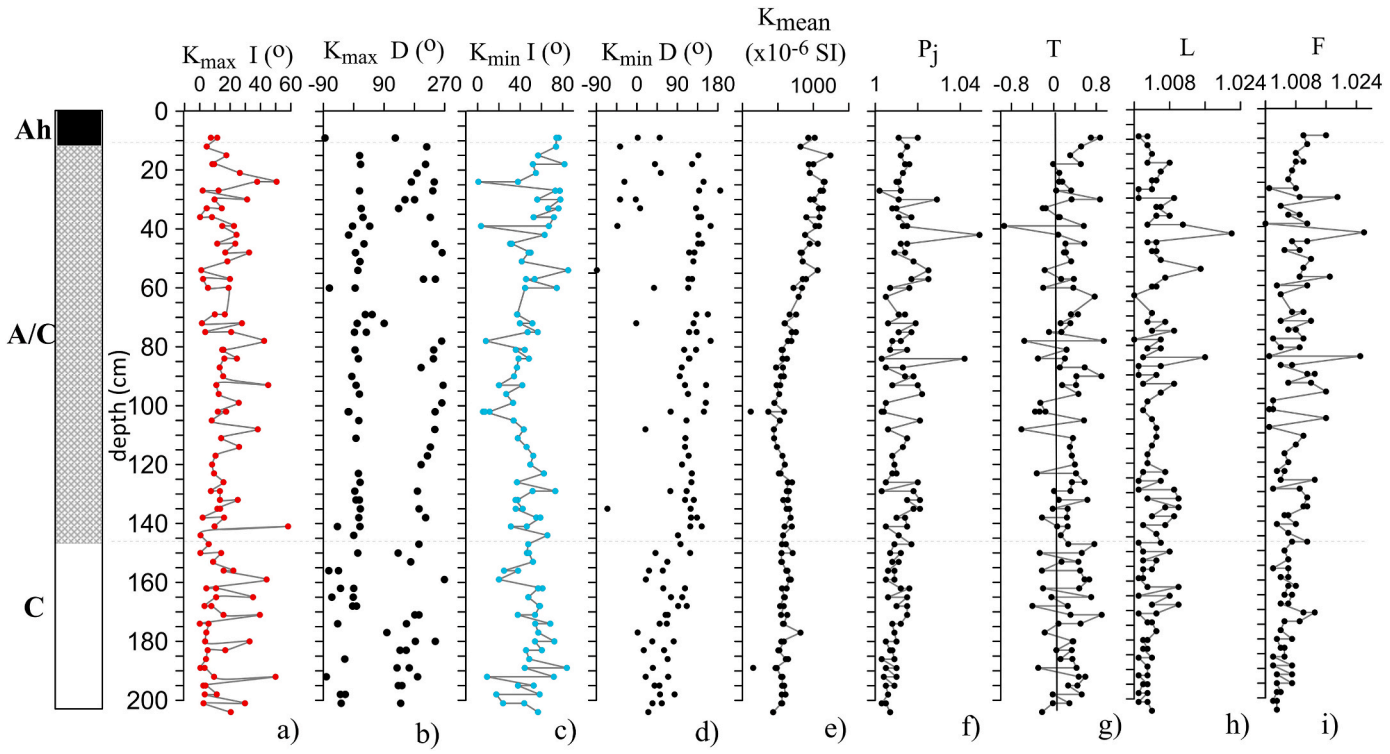

Fig. 7. Variations with depth of declination and inclination of K_{max} and K_{min} (a–d); mean volume susceptibility (K_{mean}) (e) and anisotropy parameters: corrected degree of anisotropy (Pj), shape parameter (T), lineation (L) and foliation (F).

and Barnard, 2016; Roberts et al., 2020). Its presence is further revealed by the variations with depth of the S-ratio (Fig. 4d), decreasing to 0.7 for the bottom part of the section. However, as evidenced by paleomagnetic results, this hematite is of environmental significance only and does not carry a characteristic NRM component.

The effective magnetic grain size of the magnetic phases identified can be judged by the hysteresis parameters and ratios (Fig. 4 a - c). Coercive force B_c and coercivity of remanence B_{cr} are within typical values for SD-PSD magnetites (Peters and Dekkers, 2003; Dunlop and Özdemir, 1997). Increasing proportion of high-coercivity phase in the lower part of the profile (below 100 cm depth) prevent interpretation of bulk hysteresis data in terms of domain state/grain size in this depth interval (Frank and Nowaczyk, 2008). However, the narrow interval of mean coercivity values of IRM component C2 (23.2–24.4 mT) suggests that no significant changes in the magnetic grain sizes of the magnetite/maghemite phase occur at deeper levels.

5.2. Paleomagnetic directions and relative paleointensity estimates

The choice of the best proxy for relative paleointensity record followed the main assumptions and criteria summarized by Tauxe (1993). Taking into account the results from rock magnetic data revealing the major contribution of PSD magnetite/maghemite to the bulk signal, our preferred normalizer for the NRM was ARM. Both signals were demagnetized at 20 mT for removing the viscous overprint. Comparison between ratio – derived (NRM_{20mT}/ARM_{20mT}) and slope (NRM AFdemag versus ARM AFdemag) methods for RPI estimation (Fig. 4 S) reveals similar results, better confined in the upper 140 cm of the profile. In the lower part (e.g. alluvial clays) higher discrepancy is observed, probably due to partial contribution of lower – coercivity hematite grains to the NRM signal, which did not acquire an ARM in the 100 mT peak field applied. The obtained depth records of declination, inclination and relative palaeointensity are compared with the archaeomagnetic paleosecular variation (PSV) curves for Bulgaria spanning the last 8000 y BP (Kovacheva et al., 2014). The established geomorphic position and depth of the oldest dated archaeological horizon of the Chalcolithic mound near the sampled location (being 6000 y BP at 140 cm depth) is utilized as an independent tie point in our correlation exercise, presented in Fig. 8. For each couple of archaeomagnetic time record (D, I, Fa) and depth variations of the soil sedimentary ChRM D, ChRM I and RPI' records, specific tie – points were utilized as reflected by the same colored Greek symbols. In Table 2 S these tie points are reported accordingly. Remarkable similarities are observed in the behavior of inclination and declination variations after pinning the soil depth of 140 cm–6000 y BP on the archaeomagnetic secular variation curve (Fig. 8). Apparently, there is no effect of inclination shallowing in the sedimentary record, as revealed by this comparison. On the other hand, we obtained several easterly declination values (up to 65°) in the uppermost 20 cm of the soil, which may be affected by secondary displacement. The correlation of RPI proxy to the absolute paleointensity of the Bulgarian PSV curve is reasonable except for the oldest part, where local Fa maxima at 6000 y BP is preceded by notable very wide confidence interval of the archaeomagnetic curve spanning the transitional period of Late Eneolithic – Early Bronze age (5000–6000 y BP), in which archaeomagnetic data in the Bulgarian PSV curves are scarce. Thus, the RPI maximum at 127 cm may have its analog. This would also suggest that within this period large oscillations in the paleointensity of the Earth magnetic field in the region may be present.

The resulting mean age – depth model is presented on Fig. 5S for each depth with the corresponding standard deviation. Lowest sedimentation rates are obtained for the interval 6000–4000 y BP, which subsequently increases slowly towards the recent time. Clear change in the sedimentation rate is seen at the stratigraphic boundary between alluvial clays (C horizon) and the delluvium (A/C and Ah horizons) in which soil had developed and representing the key tie point in the age model.

5.3. Paleo geomorphological reconstructions based on AMS results

Well-defined orientation of AMS ellipsoids along the studied profile reveals two distinct sedimentation regimes, leading to the development

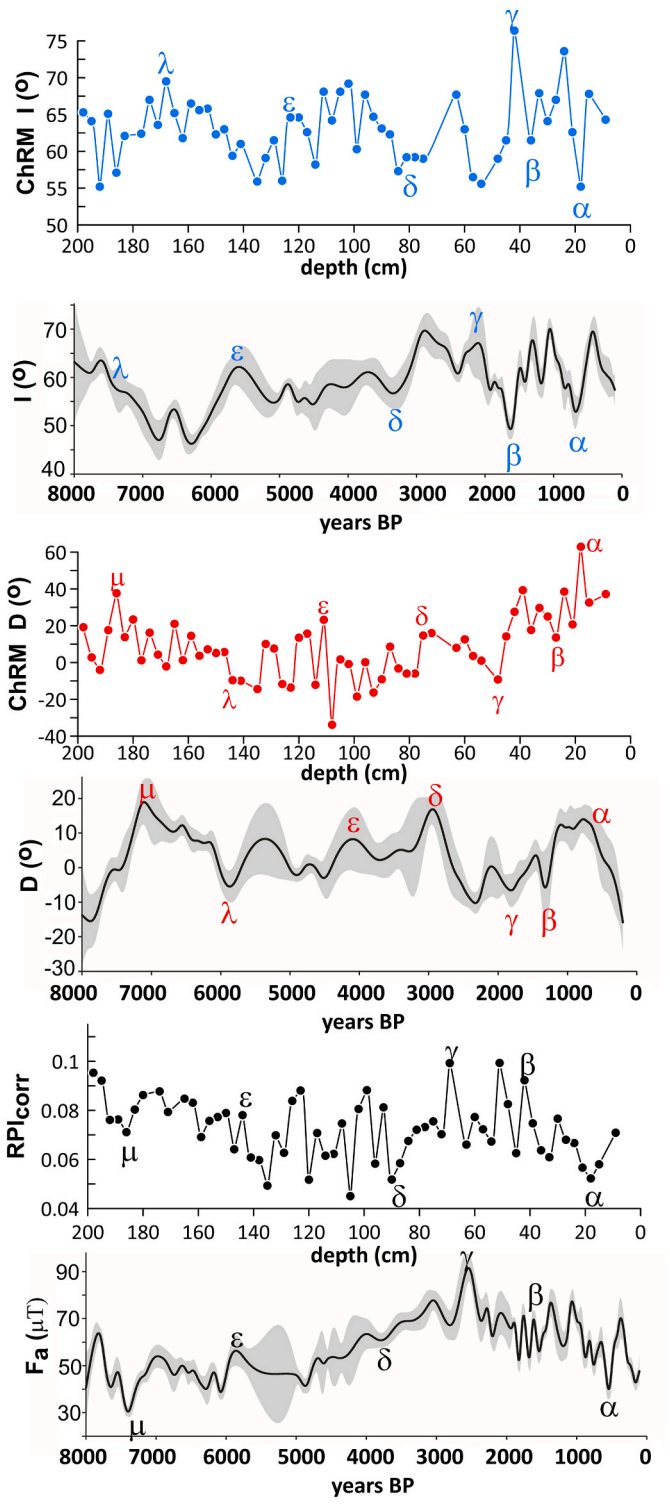

Fig. 8. Correlations between depth variations of the inclination (I) and declination (D) of the characteristic remanence (ChRM) and relative paleointensity (RPI) estimates with Bulgarian archaeomagnetic master curves (Kovacheva et al., 2014) of the secular variations of declination (D), inclination (I) and intensity (Fa) of the Earth's magnetic field for the last 8000 y BP. Tie points are marked by Greek letters of the same colour for the respective parameters compared.

of imbricated magnetic fabrics. Such imbricated fabrics are established due to the re-alignment of mineral grains with respect to the direction of the flows (air, water or magma). Under the influence of an orienting flow, particles' minimum axes steeply dip in the direction of the flow and their maximum axes are distributed in a girdle within a plane dipping in the opposite direction to transport (Bilardello, 2016).

The magnetic fabric of the soil developed in the delluvium (upper 145 cm) (Fig. 6b) exhibits an imbrication imposed by the transport of the material downslope. The direction of the transport is very well defined by the orientation of K_{min} axis. Deviating K_{min} directions with NW declinations are all pertinent to the uppermost 40 cm (see Fig. 7d) and may be influenced by recent disturbance. This fabric is a clear evidence for the transport of delluvial eroding material from the up slope. It originates from the soil cover in the region, represented by Luvisols developed on loess sediments (Evlogiev, 2006).

Alluvial clays at the bottom (146–200 cm depth) exhibit imbricated fabric with imbrication plane perpendicular to the present day orientation of the riverbed at the sampling area (Fig. 2b and c; Fig. 6c). Alignment of oblate particles in strong flow conditions may lead to grouping of K_{max} in sub-horizontal plane due to the intersection lines of the platy grains, which lie at different angle to the flow (Tarling and Hrouda, 1993; Bilardello, 2016). Higher relative contribution of hematite and lower content of strongly magnetic grains probably increases the role of clay minerals and hematite fractions in development of a composite magnetic fabric.

One interesting observation is the lag in re-orientation of the inclination of K_{min} from ~60° to shallower values (20°) and back to almost vertical close to the surface (Fig. 7 c). This change occurs at 100 cm depth, which is 45 cm higher than the observed boundary between alluvial clays and the delluvium. Similarly, rock magnetic parameters also depict clear change at 100 cm depth (Fig. 4). This would suggest that after the time of river transgression at 6000 y BP marked by the establishment of the oldest archaeological horizon of the mound, still high ground water table persisted and probably periodical flood events lead to mixed sedimentation of alluvial clays along with the major delluvial input from the slope. Starting from 100 cm upward, the mean azimuth of K_{min} direction changes from NE to SE, following the slope plunge direction (Figs. 6b and 2).

5.4. *Paleoclimatic implications of the variations in rock magnetic properties*

The obtained good quality paleomagnetic records of the three geomagnetic field elements – D, I and RPI, and the consistent AMS fabric of the studied profile suggest that the detrital fraction of the mineral magnetic carriers have distinct and stable signature. This high quality geomagnetic field recording is further predetermined by the accretional nature of the alluvial soils, whose profile develops mainly upward within the newly accumulated fluvial materials (Ferring, 2001; Alexandrovskiy, 2007). The very smooth character of bulk mass-specific magnetic susceptibility along depth of the profile (Fig. 2 S a) outlines only the gradual increase in the amount of *in situ* formed pedogenic magnetic fraction. Its increase starts at 80 cm depth, corresponding to an age of 3100 y BP. The absence of pedogenic enhancement in the sediments from 145 to 80 cm again supports the conclusion that during the Middle Holocene and the first millennia of the Late Holocene (6000–3000 y BP) (Walker et al., 2012) the terrain of the flood terrace was still not completely drained.

For deriving paleoenvironmental signal from the magnetic properties along the studied profile, we analyzed the behavior of several magnetic ratios sensitive to changes in the relative contribution of particular phase and/or grain size fraction of iron oxides.

The first paleoenvironmental magnetic proxy parameter, considered in this study is the ratio of IRM, acquired in 1T field and subsequently AF demagnetized at 20 mT (IRM_{20mT}) to the initial IRM - (IRM_{20mT}/IRM). In practice, this parameter is easily obtained as a part of the RPI estimation procedure. The rationale of using it as environmental proxy is based on the supposition that 20 mT demagnetization step eliminates magnetization of the softest magnetite like fraction, leaving the contribution of magnetically stable magnetite/maghemite and antiferromagnetic minerals. Thus, higher values of the ratio IRM_{20mT}/IRM will indicate increased relative amounts of stable magnetite like fraction plus hematite (having in mind that high-coercivity goethite would not acquire IRM in field of 1T). In an environmental context, we suppose that increased hematite content will be present in the eroding and redeposited soil, formed in a warmer climate (Cornell and Schwertmann, 2003).

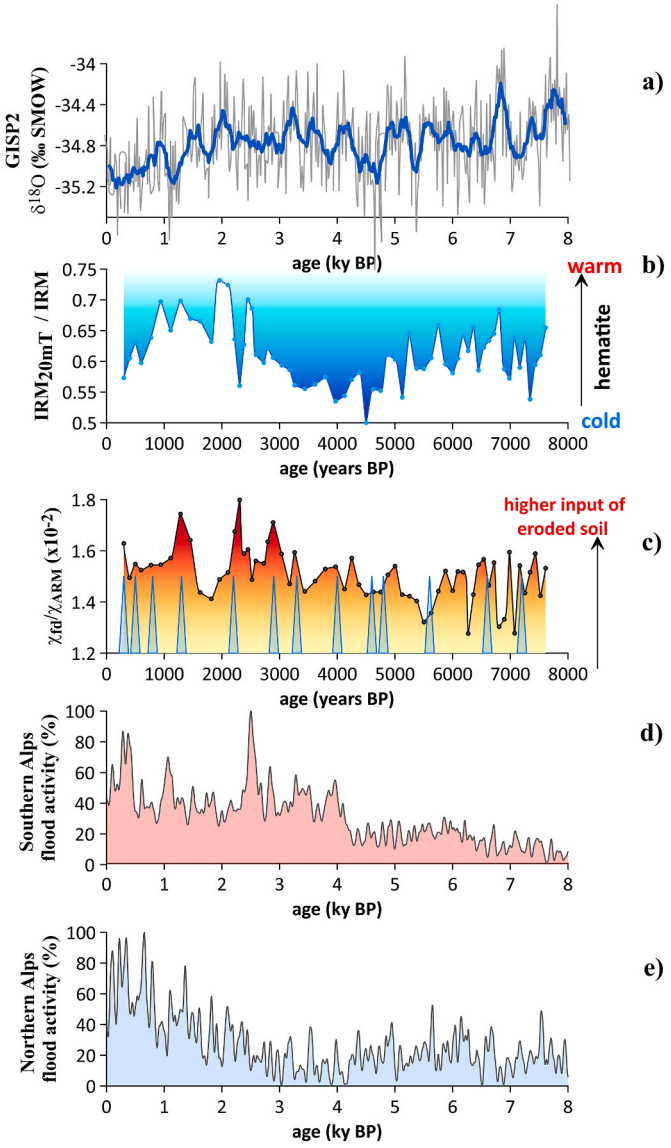

Fig. 9. Correlation of Greenland temperature record from GISP2 ice core (a) deduced from $\delta^{18}O$ variability (data from Grootes and Stuiver (1999), defined relative to standard mean ocean water (SMOW) composition with 10-points running average) with environmental proxy ratio IRM_{20mT}/IRM (b) for soil profile KP; c) Variability of χ_{fd}/χ_{ARM} ratio as compared to Southern (d) and Northern (e) Alps flood activities from Wirth et al. (2013a). Blue cones in (c) depict the timing of major flood events at Romanian Carpathian rivers according to Radoane et al. (2019). (For interpretation of the references to color in this figure legend, the reader is referred to the Web version of this article.)

Fig. 9 a, b shows the correlation of the ratio IRM_{20mT}/IRM with Greenland ice core GISP2 temperature record (Stuiver et al., 1995). Comparison between the two records reveals good correspondence between the timing of major cold events recorded in the ice core at 1.1ky, 1.8y, 4.0ky, 4.5ky, 5.4ky, 7.1ky BP with the minima in IRM_{20mT}/IRM curve (Fig. 9 a, b). Consequently, sediment fluxes during cold climate events are poorer in hematite, and conversely – fluxes during warm climate are richer in hematite. This supports our hypothesis for the soil-derived origin of the sediments and its climate – related content of pedogenic hematite fraction. The timing of the identified cold events fall within time intervals recorded in worldwide Holocene climate proxy records (Wanner et al., 2011).

The second proxy considered is the ratio between frequency dependent magnetic susceptibility (χ_{fd}) and the anhysteretic susceptibility (χ_{ARM}). Both parameters are sensitive to strongly magnetic fine grained magnetites (maghemites) with (χ_{fd}) increase upon increasing content of superparamagnetic (SP) grains (grain sizes of 12–15 nm), and χ_{ARM} increase when stable single domain grains (grain sizes of 20–25 nm) prevail (Maher, 1988). Thus, the ratio χ_{fd}/χ_{ARM} will show high values when SP fraction dominates, and low – at higher amount of particles in SD state.

Variability of χ_{fd}/χ_{ARM} along depth of the studied profile (Fig. 9c) depends on two factors. First, it is the contribution of the *in-situ* pedogenic production of SP/SD magnetites inherent to well-drained soils (Maher, 1986). In our specific case, another source of variability is the periodic flux of alluvial/delluvial material eroded from the upper slope soil cover. To test this hypothesis we compare the range of values of χ_{fd}/χ_{ARM} from the present study with data for a Luvisol (profile Koprivetz I from Jordanova et al. (1997)) located at the plateau in close proximity (~2 km to NW) and developed on loess sediments. The available data of χ_{ARM} from the past study were amended by measurements of frequency dependent susceptibility for the samples from the upper 50 cm, which encompass the humic horizon rich in organic matter and part of the lower lying transitional A/C horizon. The calculated χ_{fd}/χ_{ARM} values show good consistency and $(\chi_{fd}/\chi_{ARM})_{mean}$ of 2.146 ± 0.078 (x 10^{-2}) is obtained from 26 samples covering depth interval 0–50 cm. This value is considered as characteristic for topsoils developed on loess in the study area. Thus, the mean χ_{fd}/χ_{ARM} for loessic soils in the region is systematically higher than the variability of χ_{fd}/χ_{ARM} along the alluvial soil from the present study (Fig. 9c). Peak values reaching 1.7–1.8 (x10^{-2}) approach the one for the loessic topsoil. From this comparison we conclude that high – frequency variations in the ratio χ_{fd}/χ_{ARM} can be considered as intervals of deposition of re-worked topsoil material from the magnetically enhanced loessic soils on the plateau. The potential of magnetic method for mapping recent re-distribution and downslope deposition of eroded loessic soils has been shown in other studies (Jordanova et al., 2014; Cao et al., 2021).

The location of the studied soil profile on the floodplain of Baniska river allowed for looking at imprints of river hydrological changes in the magnetic signature. Being a tributary of the Danube River, the Baniska River comprises part of the Danube catchment and thus, its hydrology is closely related to the reaction of the Danube River system to environmental changes during the Holocene. Recent study (Martinez-Lamas et al., 2020) shows that Alpine Ice Sheet mass-balance changes are major drivers of changes in the sediment flux of the Danube rather than water level fluctuations related to the Black sea level. The main peaks in our χ_{fd}/χ_{ARM} proxy correspond well to the timing of the river floods of Romanian Carpathian rivers (Radoane et al., 2019) (blue cones in Fig. 9c). In the interval of 145–100 cm soil depth, corresponding to 6000–4100 y BP, matching of the flood events of Carpathian rivers with our proxy is not so good, probably arising from the mixing of delluvial and alluvial materials as discussed in the previous section.

Sensitivity of the environmental magnetic proxy records of Koprivetz alluvial soil to global climate change is explored by comparison of the magnetic proxy ratio χ_{fd}/χ_{ARM} with flood activity records of Southern

and Northern Alps (Wirth et al., 2013) (Fig. 9 c, d, e). Good correspondence of high χ_{fd}/χ_{ARM} values with high flood activity suggests that strong precipitation events (and/or floods) caused an increased transport of eroded topsoil material downward to the floodplain and its incorporation into the sediment column.

Wirth et al. (2013) show that strong southward migration of the westerlies and the Atlantic storm tracks during cool climate periods impose intensification of the floods activity in Southern Alps and decreased flood activity in Northern Alps. Cold climate conditions imply stronger temperature gradients between the equator and polar regions and higher frequency of extreme precipitation events at mid-latitudes (Raible et al., 2020). At the opposite, Arctic warming reduces latitudinal temperature gradients, subsequently reducing the strength and frequency of storms and related amount of annual precipitation at mid-latitudes Routson et al. (2019). The comparison of our magnetic proxy ratio to flood intensity reveals closer similarity to flood events from Southern Alps for the 4000 y BP to present time period, while older part of the χ_{fd}/χ_{ARM} proxy matches more closely the relatively stronger flood activity in Northern Alps. The shift in similarity between χ_{fd}/χ_{ARM} proxy with Southern/Northern Alps flood activity in Late/Early Holocene suggests that the climate in the region may had reacted to changing path of the westerly storm tracks. According to climate studies, westerlies migrate to the north during climate warming and are responsible for the corresponding change in precipitation (Wirth et al., 2013; Smith et al., 2016; Raible et al., 2020). Thus, a better match between our flood events magnetic proxy (χ_{fd}/χ_{ARM}) in Early Holocene to Northern Alps flood activity curve suggests that at the time of the Holocene climate optimum (6000–8000 y BP), westerlies brought increased precipitation at higher northern latitudes implying warmer climate at that time. Significantly higher maxima on χ_{fd}/χ_{ARM} after 3200 y BP until historic times implies an intensification of the flood events which may be also a result of the anthropogenic impact by forest clearance after the Bronze age (Vidal-Cordasco and Nuevo-Lopez, 2021).

6. Conclusions

The studied profile of alluvial Holocene soil near Koprivetz archaeological site in NE Bulgaria carries good quality records of both paleomagnetic direction (Declination and Inclination) and relative paleointensity for the last 8000 y BP. The good correlation of all three elements of the geomagnetic field along the profile with the archaeomagnetic paleosecular variation curves for Bulgaria allows the construction of a sound age – depth model. Temporal variations of two environmental magnetic proxy ratios - χ_{fd}/χ_{ARM} and IRM_{20mT}/IRM – show remarkable consistency with precipitation – driven paleo-flood activities in Northern and Southern Alps, and the Holocene GISP2 Greenland $\delta^{18}O$ record. Six major cold events are registered - at 1800, 2300, 4000, 4500, 5400 and 7100 y BP, well corresponding to the minima in GISP2 temperature record (Stuiver et al., 1995). The most prominent minimum is recorded at 4500 ky, probably corresponding to Bond event 3 (4800–4500 y BP) (Wanner et al., 2011). The record of increased precipitation (flooding) events revealed by χ_{fd}/χ_{ARM} in the study area exhibits maxima in the late Holocene, matching closer the record of Southern Alps flood intensity.

Data availability

Datasets related to this article will be made available at MENDELEY data repository after manuscript acceptance for publication.

CRediT authorship contribution statement

Diana Jordanova: Conceptualization, Writing – original draft, Supervision. **Bozhurka Georgieva:** Investigation, Formal analysis. **Neli Jordanova:** Writing – review & editing, Visualization, Data curation, Funding acquisition. **Yohan Guyodo:** Methodology, Resources, Writing – review & editing. **France Lagroix:** Methodology, Writing – review & editing, Funding acquisition.

Declaration of competing interest

The authors declare that they have no known competing financial interests or personal relationships that could have appeared to influence the work reported in this paper.

Acknowledgements

This work was supported by bilateral cooperation programme PHC RILA2018 (France – Bulgaria) through project KP-06-RILA/3, the corresponding project 43191 ZM of the Ministère de l'Europe et des Affaires Etrangères (MEAE) and projectKP-06-N34/2 of the Bulgarian National Science Fund.

Appendix A. Supplementary data

Supplementary data to this article can be found online at https://doi.org/10.1016/j.quaint.2022.06.009.

References

Alexandrovskiy, A., 2007. Rates of soil-forming processes in three main models of pedogenesis. Rev. Mex. Ciencias Geol. 24 (2), 283–292.
Berger, J.F., 2021. Geoarchaeological and paleo-hydrological overview of the central-western mediterranean early neolithic human–environment interactions. Open Archaeol. 7, 1371–1397.
Bilardello, D., 2016. Magnetic anisotropy: theory, instrumentation, and techniques. In: Reference Module in Earth Systems and Environmental Sciences. Elsevier Inc. https://doi.org/10.1016/B978-0-12-409548-9.09516-6
Bogucki, P., 1996. The spread of early farming in Europe. Am. Sci. 84 (3), 242–253.
Brachfeld, S., Banerjee, S.K., 2000. A new high-resolution geomagnetic paleointensity record for the North American Holocene: a comparison of sedimentary and absolute intensity data. J. Geophys. Res. 105 (B1), 821–834.
Braxmeier, 2017. Maps-for-free relief (http://www. maps-for-free.com/), (accessed 20 April 2022).
Brayshaw, D.J., Hoskins, B., Black, E., 2010. Some physical drivers of changes in the winter storm tracks over the North Atlantic and Mediterranean during the Holocene. Phil. Trans. R. Soc. A. 368, 5185–5223.
Cao, Z., Zhang, K., He, J., Yang, Z., Zhou, Z., 2021. Linking rocky desertification to soil erosion by investigating changes in soil magnetic susceptibility profiles on karst slopes. Geoderma 389, 114949.
Cornell, R., Schwertmann, U., 2003. The Iron Oxides. Structure, Properties, Reactions, Occurrence and Uses. Weinheim, New York.
Dunlop, D.J., Özdemir, Ö., 1997. Rock Magnetism: Fundamentals and Frontiers. Cambridge University Press, Cambridge, New York.
Earth, Google, 2022. Koprivets village. Available at: https://earth.google.com/web. (Accessed 19 April 2022).
Europe relief map, 2010. Wikipedia commons. https://upload.wikimedia.org/wikipedia/commons/7/79/Europe_relief_laea_location_map.jpg. (Accessed 30 May 2022).
Evlogiev, J., 2006. Plejstocenat I holocenat v dunavskata ravnina (the Pleistocene and Holocene in the Danube plain). DSc. Dissertation, Bulg. Acad. Sci. 1–272. Sofia (in Bulgarian).
Ferring, C.R., 2001. Geoarchaeology in alluvial landscapes. In: Goldberg, G., Holliday, V. T., Ferring, C.R. (Eds.), Earth Sciences and Archaeology. Springer Science + Business Media, New York, pp. 77–99.
Feurdean, A., Grindean, R., Florescu, G., Tantau, I., Niedermeyer, E.M., Diaconu, A.C., Hutchinson, S.M., Nielsen, A.B., Sava, T., Panait, A., Braun, M., Hickler, T., 2021. The transformation of the forest steppe in the lower Danube Plain of southeastern Europe: 6000 years of vegetation and land use dynamics. Biogeosciences 18, 1081–1103.
Fort, J., 2015. Demic and cultural diffusion propagated the Neolithic transition across different regions of Europe. J. R. Soc. Interface 12, 20150166.
Frank, U., Nowaczyk, N.R., 2008. Mineral magnetic properties of artificial samples systematically mixed from haematite and magnetite. Geophys. J. Int. 175 (2), 449–461.
Grootes, P.M., Stuiver, M., 1999. GISP2 oxygen isotope data. PANGAEA Database. https://doi.org/10.1594/PANGAEA.56094.
Guo, H., Barnard, A.S., 2016. Thermodynamics of iron oxides and oxyhydroxides in different environments. In: Faivre, D. (Ed.), Iron Oxides: from Nature to Applications. VCH Verlag GmbH & Co., pp. 269–292
Hanesch, M., Stanjek, H., Petersen, N., 2006. Thermomagnetic measurements of soil iron minerals: the role of organic carbon. Geophys. J. Int. 165, 53–61.
Hrouda, F., 1982. Magnetic anisotropy of rocks and its application in geology and geophysics. Geophys. Surv. 5, 37–82.
Jelinek, V., 1981. Characterization of the magnetic fabric of rocks. Tectonophysics 79, 63–67.

Jiang, Z., Liu, Q., Zhao, X., Jin, C., Liu, C., Li, S., 2015. Thermal magnetic behaviour of Al-substituted haematite mixed with clay minerals andits geological significance. Geophys. J. Int. 200, 130–143.
Jordanova, D., Petrovsky, E., Jordanova, N., Evlogiev, J., Butchvarova, V., 1997. Rock magnetic properties of recent soils from North Eastern Bulgaria. Geophys. J. Int. 128, 477–484.
Jordanova, D., Jordanova, N., Petrov, P., 2014. Pattern of cumulative soil erosion and redistribution pinpointed through magnetic signature of Chernozem soils. Catena 120, 46–56.
King, J., Channell, J.E.T., 1991. Sedimentary magnetism, environmental magnetism, and magnetostratigraphy. In: U.S. National Report to the International Union of Geodesy and Geophysics, vol. 29. AGU, Washington, D. C, pp. 358–370.
Kovacheva, M., Kostadinova-Avramova, M., Jordanova, N., Lanos, Ph, Boyadzhiev, Y., 2014. Extended and revised archaeomagnetic database and secular variation curves from Bulgaria for the last eight millennia. Phys. Earth Planet. In. 23, 79–94.
Lagroix, F., Banerjee, S.K., 2004. The regional and temporal significance of primary aeolian magnetic fabrics preserved in Alaskan loess. Earth Planet Sci. Lett. 225, 379–395.
Macklin, M.G., Lewin, J., Woodward, J.C., 2012. The fluvial record of climate change. Phil. Trans. R. Soc. A 370, 2143–2172.
Maher, B., 1986. Characterization of soils by mineral magnetic measurements. Phys. Earth Planet. In. 42, 76–92.
Maher, B.A., 1988. Magnetic properties of some synthetic sub-micron magnetites. Geophys. J. 94, 83–96.
Martinez-Lamas, R., Toucanne, S., Debret, M., Riboulot, V., Deloffre, J., Boissier, A., Cheron, S., Pitel, M., Bayon, G., Giosan, L., Soulet, G., 2020. Linking Danube River activity to Alpine Ice-Sheet fluctuations during the last glacial (ca. 33–17 ka BP): insights into the continental signature of Heinrich Stadials. Quat. Sci. Rev. 229, 106136.
Maxbauer, D.P., Feinberg, J.M., Fox, D.L., 2016. MAX UnMix: a web application for unmixing magnetic coercivity distributions. Comput. Geosci. 95, 140–145.
Murad, E., Wagner, U., 1998. Clays and clay minerals: the firing process. Hyperfine Interact. 117, 337–356.
Peters, C., Dekkers, M.J., 2003. Selected room temperature magnetic parameters as a function of mineralogy, concentration and grain size. Phys. Chem. Earth 28, 659–667.
Ponomar, V.P., AntonenkoT, S., Vyshnevskyi, O.A., Brik, A.B., 2020. Thermally induced changes in the magnetic properties of iron oxide nanoparticles under reducing and oxidizing conditions. Adv. Powder Technol. 31 (7), 2587–2596.
Popov, V., 1996. Periodizacia I hronologia na neolitnite I halkolitni kulturi v porechieto na r. Rusenski Lom. In: (Periodization and Chronology of the Neolithic and Chalcolithic Cultures from the Valley of Russenski Lom River. State Archives, Russe, 954-1839-03-X.
Radoane, M., Chiriloaei, F., Sava, T., Nechita, C., Radoane, N., Gaza, O., 2019. Holocene fluvial history of Romanian Carpathian rivers. Quat. Int. 52, 113–129.
Raible, C.C., Pinto, J.G., Ludwig, P., Messmer, M., 2020. A review of past changes in extratropical cyclones in the northern hemisphere and what can be learned for the future. WIREs Clim Change, e680.
Roberts, A.P., Zhao, X., Heslop, D., Abrajevitch, A., Chen, Y.-H., Hu, P., Jiang, Z., Liu, Q., Pillans, B.J., 2020. Hematite (α-Fe2O3) quantification in sedimentary magnetism: limitations of existing proxies and ways forward. Geosci. Lett. 7–8. https://doi.org/10.1186/s40562-020-00157-5.
Routson, C.C., McKay, N.P., Kaufman, D.S., Erb, M.P., Goosse, H., Shuman, B.N., Rodysill, J.R., Ault, T., 2019. Mid-latitude net precipitation decreased with Arctic warming during the Holocene. Nature 568, 83–87.
Ruddiman, W.F., Fuller, D.Q., Kutzbach, J.E., Tzedakis, P.C., Kaplan, J.O., Ellis, E.C., Vavrus, S.J., Roberts, C.N., Fyfe, R., He, F., Lemmen, C., Woodbridge, J., 2016. Late Holocene climate: natural or anthropogenic? Rev. Geophys. 54 (1), 93–118.
Smith, A.C., Wynn, P.M., Barker, P.A., Leng, M.J., Noble, S.R., Tych, W., 2016. North Atlantic forcing of moisture delivery to Europe throughout the Holocene. Sci. Rep. 6, 24745.
Stoner, S.J., St-Onge, G., 2007. Magnetic stratigraphy in paleooceanography: reversal, excursion, paleointensity and secular variation. In: Hillaire-Marcel, C., de Vernal, A. (Eds.), Proxies in Late Cenozoic Paleoceanography. Elsevier, pp. 99–138.
Stuiver, M., Grootes, P.M., Braziunas, T.F., 1995. The GISP2 deltaO-18 climate record of the past 16,500 years and the role of the sun, ocean,and volcanoes. Quat. Res. 44, 341–354. https://doi.org/10.1006/qres.1995.1079.
Tarling, D.H., Hrouda, F., 1993. The Magnetic Anisotropy of Rocks. Chapman & Hall, London, p. 217.
Tauxe, L., 1993. Sedimentary records of relative paleointensity of the geomagnetic field: theory and practice. Rev. Geophys. 31 (3), 319–354.
Tauxe, L., Wu, G., 1990. Normalized remanence in sediments of the Western Equatorial Pacific: relative paleointensity of the geomagnetic field? J. Geophys. Res. 95 (B8), 12337–12350.
Till, J.L., Guyodo, Y., Lagroix, F., Ona-Nguema, G., Brest, J., 2014. Magnetic comparison of abiogenic and biogenic alteration products of lepidocrocite. Earth Planet Sci. Lett. 395, 149–158.
Till, J.L., Guyodo, Y., Lagroix, F., Morin, G., Ona-Nguema, G., 2015. Goethite as a potential source of magnetic nanoparticles in sediments. Geology 43 (1), 75–78.
Vidal-Cordasco, M., Nuevo-Lopez, A., 2021. Resilience and vulnerability to climate change in the Greek Dark Ages. J. Anthropol. Archaeol. 61, 101239.
Walker, M.J.C., Berkelhammer, M., Bj€orck, S., Cwynar, L.C., Fisher, D.A., Long, A.J., Lowe, J.J., Newnham, R.M., Rasmussen, S.O., Weiss, H., 2012. Formal subdivision of the Holocene series/epoch: a discussion paper by a working group of INTIMATE (integration of ice-core, marine and terrestrial records) and the subcommission on quaternary stratigraphy (international commission on stratigraphy). J. Quat. Sci. 27, 649–659.
Wanner, H., Solomina, O., Grosjean, M., Ritz, S.P., Jetel, M., 2011. Structure and origin of Holocene cold events. Quat. Sci. Rev. 30, 3109–3123.
Weninger, B., Clare, L., Rohling, E., Bar-Yosef, O., Böhner, U., Budja, M., Bundschuh, M., Feurdean, A., Gebe, H.G., Jöris, O., Linstädter, J., Mayewski, P., Mühlenbruch, T., Reingruber, A., Rollefson, G., Schyle, D., Thissen, L., Todorova, H., Zielhofer, C., 2009. The impact of rapid climate change on prehistoric societies during the Holocene in the eastern mediterranean. Documenta Praehistorica 36, 7–59. https://doi.org/10.4312/dp.36.2.
Weninger, B., Clare, L., Gerritsen, F., Horejs, B., Krauß, R., Linstädter, J., Özbal, R., Rohling, I.J., 2014. Neolithisation of the aegean and southeast Europe during the 6600–6000 cal BC period of rapid climate change. Documenta Praehistorica XLI. https://doi.org/10.4312/dp.41.1.
Wirth, S.B., Glur, L., Gilli, A., Anselmetti, F.A., 2013. Holocene flood frequency across the Central Alps - solar forcing and evidence for variations in North Atlantic atmospheric circulation. Quat. Sci. Rev. 80, 112–128. https://doi.org/10.1016/j.quascirev.2013.09.002.
Wirth, S.B., Glur, L., Gilli, A., Anselmetti, F.A., 2013a. Holocene flood activity data for the Northern and Southern Central Alps reconstructed from lake sediments. PANGAEA. https://doi.org/10.1594/PANGAEA.823415.
Zhu, R., Liu, Q., Jackson, M.J., 2004. Paleoenvironmental significance of the magnetic fabrics in Chinese loess-paleosols since the last interglacial (<130 ka). Earth Planet Sci. Lett. 221, 55–69.